Dynamic floral scent profile of *Epiphyllum oxypetalum* and the cytosolic biosynthesis of trans-Geraniol through mevalonate pathway

Yiyang Zhang [1, *], Yuhan Zhang [1, *], Qiurui Tian [1], Likun Wei [1], Wei Tang [2], Ting Zhu [1], Zhiwei Zhou [1], Jiaqi Wang [1], Haijun Xiao [1], Zhibin Liu [1], Tao Li [1], Qun Sun [1]

[1] Key Laboratory of Bio-resources and Eco-environment Ministry of the Education, College of Life Sciences, Sichuan University, Chengdu, Sichuan 610064, PR China

[2] Sichuan Academy of Botanical Engineering, Sichuan Academy of Agricultural Sciences, Zizhong, Sichuan 641200, PR China

Authors for correspondence:

Qun Sun: qunsun@scu.edu.cn

Tao Li: tao.li@scu.edu.cn

[*] These authors contributed equally to this work

Total word count (excluding summary, References and legends):	4646	No. of figures:	8 figures (Fig. 1-8 in colour)
Summary	170	No. of Tables:	3
Introduction	646	No. of Supporting Information files:	0
Materials and methods	1737		
Results	1562		
Discussion	857		
Acknowledgements:	46		

ORCID：

Qun Sun, https://orcid.org/0000-0002-4372-8865

Yiyang Zhang, https://orcid.org/0000-0002-2159-6451

Yuhan Zhang, https://orcid.org/0009-0009-3562-2452

Qiurui Tian, https://orcid.org/0009-0002-3782-5594

Haijun Xiao, https://orcid.org/0000-0002-9587-8101

Summary

- *Epiphyllum oxypetalum*, a renowned ornamental species in Cactaceae, unveils its attractive fragrance during its infrequent and rapid night blooming. However, the nature of this floral scent remains unexplored.
- Employing GC-MS, transcriptome and biochemical assay, we systematically characterized the composition, emission dynamics and biosynthesis of *E. oxypetalum* floral scent.
- Composition of the floral scent was highly dynamic, with 72.54% trans-Geraniol, 12.96% benzyl alcohol and 3.75% methyl salicylate at full bloom. From 22:00 to 05:00 the following day, the strong scent was primarily released from petals and sepals. Proved by inhibitor assay, the precursors for the dominant scent volatile trans-Geraniol are derived from amyloplast degradation and mevalonate (MVA) pathway. Together with the cytosol-localized geraniol pyrophosphate synthase *EoGDPS* and geraniol synthase *EoTPSa1*, we proved an uncanonical cytoplasmic biosynthesis route for monoterpene volatiles in *E. oxypetalum* petal.
- Our study on the dynamic floral scent profile and its biosynthesis posed the first detailed analysis of cactus floral scent. These results laid foundation for novel perfume development and future inquiries on specialized pollination coevolution in Cactaceae.

Key words: floral scent, VOCs, emission dynamics, transcriptome, terpene biosynthesis.

41 **1. Introduction**

42 Angiosperm flowers emit a diverse and complex bouquet of volatile organic compounds
43 (VOCs), which consist primarily of terpenoids, amino-acid derived aromatics and fatty-acid
44 derivatives (Dudareva et al., 2013). Since the first report of orchid scent in 1966 (Dodson & Hills,
45 1966), thousands of compounds have been identified as floral VOCs by gas chromatography mass
46 spectroscopy (GC-MS) and related techniques (Knudsen *et al.*). The composition and emission
47 patterns of floral VOCs exhibit considerable spatial and temporal variability (Zhang *et al.*, 2022),
48 giving rise to distinct and characteristic fragrance across different species (Knudsen *et*
49 *al.*) ,(Parachnowitsch *et al.*, 2012). Floral VOCs play a crucial role in plant-insect interactions
50 (Sachse & Galizia, 2003; Heiling, 2004; Eltz *et al.*, 2005), including pollinator attraction (Tan &
51 Nishida, 2007) and nectar repellent, thereby significantly contributing to plant reproduction and
52 evolution (Raguso, 2008). Furthermore, floral VOCs hold immense importance in the cosmetic
53 and fragrance industries, creating substantial economic value (Chen & Viljoen, 2010).

54 From a biosynthetic perspective, terpenoids constitute the most abundant group of floral
55 VOCs, with more than 40,000 different compounds documented (Abbas *et al.*, 2017). They are
56 typically synthesized through two distinct pathways, i.e., the cytosol-localized mevalonate (MVA)
57 pathway and the plastid-localized 2-C-methyl-D-erythritol-4-phosphate (MEP) pathway
58 (Muhlemann *et al.*, 2014), Both pathways synthesize the fundamental C_5 building blocks for
59 terpenoid biosynthesis, namely isopentyl pyrophosphate (IPP) and dimethylallyl pyrophosphate
60 (DMAPP). These building blocks are subsequently condensed repeatedly by prenyltransferases
61 into isoprenoid pyrophosphates of varying lengths (Chang *et al.*, 2006). Finally, terpene synthases
62 (TPSs) catalyze the conversion of these pyrophosphates into the corresponding terpene skeletons
63 (Chen *et al.*, 2011). The biosynthesis of terpenoids is predominantly governed by TPSs utilizing
64 the Class-I mechanism, characterized by conserved Mg^{2+} or Mn^{2+} binding DDxxD and NSE/DTE
65 motifs (Christianson, 2017). This mechanism, along with subsequent modifications, enables the
66 diverse rearrangement of terpenoids, resulting in their remarkable structural diversity (Qiao *et al.*,
67 2021).

68 In higher plants, the MEP pathway generally provides substrates for monoterpenes (C_{10}) and
69 diterpenes (C_{20}) production, while the MVA pathway supplies substrates for sesquiterpene (C_{15})

70 and triterpene (C_{30}) biosynthesis. However, emerging evidence suggests that metabolic crosstalk
71 between the two terpenoid biosynthesis pathways occurs more frequently than currently
72 established. For instance, studies using isotope-labeled precursors have indicated that the MEP
73 pathway may participate in sesquiterpene formation in cotton seedlings (Opitz *et al.*, 2014).
74 Similar metabolic crosstalk has been observed in snapdragon flowers, where the MEP pathway
75 provides C_5 precursors for both monoterpene and sesquiterpene biosynthesis (Dudareva *et al.*,
76 2005). While most ultrastructural studies have demonstrated the plastid localization of
77 monoterpene-producing TPSs, there have been a few cases suggesting cytosolic monoterpene
78 biosynthesis utilizing C_5 precursors derived from the MEP pathway (Schuhr *et al.*, 2003;
79 'Dynamic pathway allocation in early terpenoid biosynthesis of stress-induced lima bean leaves',
80 2006; Gutensohn *et al.*, 2013; Opitz *et al.*, 2014; Mendoza-Poudereux *et al.*, 2015), However,
81 documentation of cytosol-localized monoterpene biosynthesis remain limited in the literature.

82 Previous studies have reported floral VOC emission patterns in several cactus species, such
83 as *Selenicereus grandiflorus* and *Pilosocereus arrabidae*, etc.(Kaiser & Tollsten, 1995), the
84 emission dynamics of floral VOCs in *E. oxypetalum* and the underlying molecular mechanisms
85 remain unexplored. Considering the impressive rhythm of blooming that *E. oxypetalum* displays,
86 in-depth researches on synthesis of its flower fragrance can contribute to our comprehension of the
87 rapid production of aroma compound in plants and the physiological transformations that take
88 place during flowering. This research can also stimulate ideas for genetic editing-based breeding.
89 Furthermore, it has the potential to offer substantial economic benefits by facilitating the
90 development of new spices and essences, thereby providing a competitive advantage to related
91 industries. In this study, leveraging the excellent germplasm resources, we firstly unveiled a
92 remarkable physiological phenomenon in *E. oxypetalum* flowers, demonstrated that the explosive
93 emission of flower fragrance was predominantly composed of monoterpenoids, which were
94 synthesized within the cytoplasm of the petals during the flowering stage, contrary to the
95 previously accepted notion.

96 ## 2. Materials and methods

97 ### 2.1 Plant materials and chemicals

98 Plant materials of *E. oxypetalum* were collected from 5-years old cottage seedlings at the *E.*
99 *oxypetalum* planting demonstration base of Sichuan Yuanlan Agricultural Development Co., Ltd.
100 in Zizhong, Sichuan, China (29°40′N, 104°45′E). The seedlings were grown under semi-natural
101 conditions with soil enriched with pine needle mulch soil. To aid in the development of healthy
102 flowers, a specialized phosphate-potash-amino acid mixture was applied as a foliar fertilizer
103 before bud formation. Shade roofs were used during the summer to protect plants from excessive
104 sunlight, which could potentially cause sun scorching and negatively impact flower formation. For
105 RNA-seq, qRT-PCR molecular cloning and biochemical experiments, Samples from various parts
106 of the flowers were collected in September, immediately frozen in liquid nitrogen and stored at
107 -80℃. The materials used for SPME-GC/MS were collected into glass headspace bottles,
108 immediately frozen and stored in dry ice. Floral scent volatile samples for DHC-GC/MS were
109 collected in October with headspace adsorption.. All chemical reagents used were purchased from
110 Aladdin.

111 ### 2.2 Floral VOC collection and GC-MS analysis

112 For *in situ* VOC collection, the floral scent *E. oxypetalum* was sampled hourly from 19:00
113 p.m. to 7:00 a.m. the following day using a push-pull headspace sampling system. Briefly,
114 precleaned (120℃ for 1h) polyethylene terephthalate (PET) bags (35 × 43 cm) were securely
115 attached to the pedicel to enclose the flower. Filtered air was circulated through the bag at a flow
116 rate of 1,000 ml min^{-1} using a battery-operated pump connected to Teflon tubing. The incoming air
117 was purified by an activated charcoal filter to remove particles and VOCs, and a coper tube coated
118 with potassium iodide to scrub for ozone. Air was sucked out of the bag at a flow rate of 200 ml
119 min^{-1} through a stainless-steel adsorbent cartridge. VOCs were collected from three flowers, each

120 from a different plant. After sampling, cartridges were sealed with Teflon-coated brass caps and
121 stored at 4℃ until analysis. Blank measurements from empty PET bags were done to characterize
122 impurities originating from sampling or analysis system.

123 VOCs trapped in adsorbent cartridges were thermally desorbed (TD100-xr, Markes
124 International Ltd, Llantrisant, UK) at 250℃ for 10 min and analyzed on a gas
125 chromatograph-mass spectrometer (7890A GC, 5975C VL MSD, Agilent Technologies, Santa
126 Clara, California, USA). The VOCs were first cryofocused at -10 ℃ and then injected into
127 HP-5MS capillary column (30 m × 0.2 mm, film thickness 0.25 μm), using helium as carrier gas at
128 flow rate of 1.0 ml min^{-1} with temperature program as follows: 40℃, held 1 min; raised at 5℃
129 min^{-1} to 210℃, raised at 20℃ min^{-1} to 250℃, held 8 min.

130 For flower organ VOC extraction, VOCs were sampled using SPME fiber (SUPELCO
131 57328-U, PDMS) for 40 min at 50 ℃. VOCs adsorbed by SPME fibers were thermally desorbed
132 at 230 ℃ before analyzed on a gas chromatograph-mass spectrometer (SHIMADZU
133 GCMS-QP2010). Helium was used as carrier gas at flow rate of 1.0 ml min^{-1} using temperature
134 program as follows: 50 ℃, held 3 min; raised at 6 ℃ min^{-1} to 200 ℃, raised at 10 ℃ min^{-1} to
135 240 ℃, held 6 min.

136 Chromatograms were analyzed using PARADISe v.6.0.1 (Quintanilla-Casas *et al.*, 2023).
137 Compounds were identified using pure standards when available, or tentatively identified using
138 NIST17 library. VOCs were categorized into the following classes: terpenoids; fatty-acid
139 derivatives; benzenoids alcohols and others which do not fall within the aforementioned categories.
140 The VOC concentrations in blanks were subtracted from those in the samples.

141 **2.3 Inhibitor assay for MVA and MEP pathways**

142 In the inhibitor experiment, we administered 100μM solution of inhibitors (fosmidomycin for
143 MEP or mevinolin for MVA (Dudareva *et al.*, 2005)) by uniformly injecting 1ml of the solution
144 into the junction of petals and perianth tubes at three specific time points: Stage2, Stage3, and
145 Stage4. The control group received H_2O through injection. The needle was inserted into the cavity
146 at the center of the flower during injection, and approximately 0.1ml of liquid droplets was
147 injected per insertion. Throughout the experiment, the chosen inhibitors did not cause any

148 noticeable effects on the appearance of the flowers. For MVA inhibitor assay, lactone hydrolysis
149 were done following previous report (Kita *et al.*, 1980).

150 **2.4 RNA-seq and analysis**

151 Total RNAs were extracted from *E. oxypetalum* petal using improved hexadecyl trimethyl
152 ammonium bromide (CTAB) method. Three replicates of DNBSEQ RNA-seq libraries were
153 prepared and quality-checked from petal at each sampling stages: pre-Bloom (9:00 a.m.),
154 Blooming (S06) and post-Bloom (S13). These nine libraries were sequenced using the
155 MISEQ-2000 platform by BGI, resulting in 150 bp paired-end reads. Subsequently, the raw
156 sequencing reads underwent quality control and cleaning (Bolger *et al.*, 2014), involving the
157 removal of adaptors, ambiguous N-containing reads, and low-quality reads. The resulting clean
158 data were then *de novo* assembled into transcripts using Trinity (Grabherr *et al.*, 2011; Haas *et al.*,
159 2013).

160 For sequence annotation, all assembled transcripts were compared to NCBI Nr, swiss-prot,
161 GO (The Gene Ontology Consortium *et al.*, 2023) and KEGG databases (Kanehisa & Goto, 2000)
162 with E-value threshold at $1e^{-5}$ for BLAST operations (Altschul *et al.*, 1990). Pfam protein database
163 (Mistry *et al.*, 2021) was searched using HMMER program (Eddy, 2011) with E-value threshold
164 set at $1e^{-5}$. Annotation integration and functional categorization by GO terms was performed by
165 Trinotate (Duarte *et al.*, 2021). Later, abundance estimation and TMM (Trimmed mean of
166 M-values) was calculated by RSEM (Li & Dewey, 2011). A false discovery rate (FDR) < 0.01 and
167 absolute value of $\log_2$ratio≥2 was used to identify differentially expressed genes with DESeq2
168 (Love *et al.*, 2014). GO term enrichment was implemented by GOseq R package (Young *et al.*,
169 2010) based on Wallenius non-central hyper-geometric distribution. MUSCLE (Edgar, 2004),
170 ModelTest-NG (Darriba *et al.*, 2020), RAxML-NG (Kozlov *et al.*, 2019) and iTOL (Letunic &
171 Bork, 2021) were used for sequence clustering.

172 **2.5 QRT-PCR for genes responsible for trans-Geraniol synthesis**

173 Specific primers for qRT-PCR were designed with NCBI. Total RNAs were extracted from *E.*
174 *oxypetalum* petals with Sangon biotech Plant Total RNA Isolation Kit (Sangon company,
175 https://www.sangon.com). Full-length cDNA was then reverse transcribed using Takara Prime

176 Script™ RT reagent Kit (Perfect Real Time) (https://www.takarabiomed.com.cn). qRT-PCR was
177 performed with Takara. RR430B TB Green Fast qPCR system, using independent RNA
178 preparations as biological replicates. Ubqln gene transcripts were used as control. The relative
179 expression levels of target genes were calculated by $2^{-\Delta\Delta Ct}$. The specificity of each primer pair was
180 verified by agarose gel electrophoresis, melting curve analysis and sequence homology with local
181 script. All relevant primer sequences were given in Table 3.

182 **2.6 Cloning of *EoTPSa1* and *EoGDPS* cDNA**

183 On the basis of the transcriptome data, the primers were designed to amplify sectional cDNA
184 fragment with Takara PrimeSTAR® Max PCR system. Putative *EoTPSa1* and *EoGDPS*
185 sequence were blasted against transcriptome assembly and aligned by MUSCLE (Edgar, 2004).
186 Structure prediction and molecular docking of *EoTPSa1* were established with Alphafold2
187 (Jumper *et al.*, 2021) and AutoDock (Morris *et al.*, 2009).

188 **2.7 *Escherichia coli* expression and purification of *EoTPSa1***

189 For *in vitro* enzymatic analysis, cDNA of *EoTPSa1* was amplified and ligated into the
190 multiple cloning sites of pET-28a expression vector utilizing Takara. In-Fusion Snap Assembly
191 Master Mix. The construct was later transformed into *E. coli Rosseta-gami 2 (DE3)*. Positive
192 clones were incubated at 37 ℃ with 200 rpm shaking overnight in LB liquid medium
193 supplemented with 100 μg/ml kanamycin. After diluted to OD_{600nm} between 0.3 and 0.4, 1mM
194 isopropyl-β-D thiogalactopyranoside (IPTG) was added into culture medium to induce protein
195 expression. *E. coli* culture was incubated at 37 ℃ for 4 hours and centrifuged at 8000g for 8 min
196 before extracting total protein with Bacterial Protein Extraction Kit (Sangon). The crude protein
197 was purified by Ni-NTA spin columns (Sangon) according to manufacturer's instructions. Purified
198 *EoTPSa1* protein was examined by 12.5% (w/v) sodium dodecyl sulfate-polyacrylamide gel
199 electrophoresis (SDS-PAGE).

200 **2.8 The *in vitro* enzyme activity assay of *EoTPSa1***

201 The enzymatic assay was conducted in 0.5ml reaction buffer (50 mM Tris–HCl, 1 mM $MgCl_2$,
202 0.1 mM $MnCl_2$) supplemented with 100 μM of geranyl diphosphate. Later, 0.5μg of purified
203 *EoTPSa1* protein was added into reaction buffer. After overlaid with 100μl hexane, the reaction

204 mixtures were incubated at 21 ℃ for 1 min. Reaction products were extracted by vertexing
205 vigorously for 10s, keeping on ice for 30, and centrifugation at 12000×g for 30s at 4 ℃ to separate
206 supernatant hexane. 10μl of the dehydrated hexane supernatant was collected for GCMS analysis.
207 Product verification and quantification was achieved by comparison with NIST17 library and
208 authentic standards.

209 **2.9 Subcellular localization assay of EoTPSa1 and EoGDPS**

210 The protocol for transient gene expression in *N. benthamiana* was conducted according to
211 established procedures. In brief, both pSuper1300-EoTPSa1 and pSuper1300-EoGDPS were
212 constructed by Takara. In-Fusion Snap Assembly Master Mix and transformed into the
213 *Agrobacterium* strain GV3101. The *Agrobacteria* strains were cultured overnight in LB until their
214 OD_{600} reached 0.6. They were then collected and resuspended in induction medium (LB, 100 mM
215 acetosyringone) with their OD_{600} adjusted to 0.4. Transfection was carried out using a 1 ml
216 needle-less syringe into the leaves of one-month-old *N. benthamiana* plants. Following infiltration,
217 the plants were kept in the dark for 24 hours.

218 **2.10 Transmission electron microscopy assay**

219 *E. oxypetalum* petal samples were prefixed with a 3% glutaraldehyde. Tissues for TEM
220 examination was then postfixed in 1% osmium tetroxide, dehydrated in serial acetone, serial
221 infiltrated and embedded with Epox 812 resin. The semithin sections were stained with methylene
222 blue. Ultrathin sections were cut with diamond knife and stained with uranyl acetate and lead
223 citrate. Sections were examined with JEM-1400-FLASH Transmission Electron Microscope
224 (JEOL Ltd.).

225 **2.12 Biochemical characterization of the acetyl-CoA generating metabolic pathway**

226 The samples were collected from petals on T01-T08 (9:00 a.m. the day before bloom; 9:00
227 p.m. the day before bloom; 9:00 a.m.; 12:00 p.m.; 7:00 p.m.; 0:00 a.m. the next day; 9:00 a.m. the
228 next day; 12:00 p.m. the next day). The biochemical experiments were conducted using reagent
229 kits purchased from Sangon Biotech company: reducing sugar (D799393), triglyceride (D799795),
230 free fatty acids (D799793), and acetyl-CoA (D751001). Amylum and soluble polysaccharides
231 were separated via centrifugation at 10krpm for 10 minutes after the homogenization. Amylum

232 was washed with ddH_2O, while soluble polysaccharides were precipitated using 80% ethanol
233 afterwards. Both components were then tested with the Amylum Content Assay Kit (D799325).
234 Absorbance in each well was measured at a wavelength of required using an Agilent BioTek
235 Synergy H1 Multimode Reader.

236 ## 3. Results

237 ### 3.1 The dynamic scent composition of *E. oxyptalum*

238 Unlike many other plant species that bloom gradually over an extended period, *E.*
239 *oxypetalum* flowers rapidly transform into magnificent, fully opened flowers (Fig. 1a, Video S1).
240 The flowers typically open after 20:00 local time, and reach their full bloom after around 23:00,
241 within a short period of 3 hours (Fig. 1b). We sampled a total of 13 stages of floral VOCs sample
242 from 19:00 to 07:00 the next day with the dynamic headspace collection technique, covering
243 entire scent emission which increase simultaneously with flower opening shortly after sunset (Fig.
244 1c, 1f). In total, we identified 49 compounds, including 26 terpenoids, 5 fatty acid derivatives and
245 18 benzenoids VOCs. Of all these VOCs, 3 particular VOCs were detected with highest content,
246 namely trans-Geraniol, Benzyl alcohol and Methyl salicylate. At 02:00 local time (Stage 08) when
247 *E. oxypetalum* flower reaches highest emission, these 3 VOCs constitutes 90.25% of total detected
248 volatile emission (trans-Geraniol, 72.54%; Benzyl alcohol, 13.72%; Methyl salicylate, 4.55%, ,
249 Table 1, 2, Fig. 1d). Multivariate OPLS-DA statistics also identified them as best variables
250 separating blooming and non-blooming VOC composition (Fig. 1e). Therefore, we identified these
251 as major *E. oxypetalum* floral scent VOCs.

252 Significant volatile content and composition were observed at each stage (Fig. 1d). From
253 20:00 to 02:00 (stage 03 and 08), emission rate of scent volatiles increased 47 times in a short 6
254 hours, with peak emission rate of 165.45 μg/flower/h at 02:00 (Stage 08). Initially, esters
255 constitute the dominant VOCs, accounting for 92.46% of the total emission shortly after the
256 initiation of scent emission at 21:00 (Stage 03). Terpenoids began to emit at 20:00. (Stage 04),
257 gradually becoming the dominant VOC class at 01:00 (Stage 07), constituting 81.33% of the total
258 emission. Concurrent with the terpenoid emission increase, benzenoid alcohols gradually
259 surpassed benzenoid esters as the primary benzenoid VOCs, reaching their peak emission at 03:00
260 (Stage 09), slightly after the terpenoid peak. Subsequently, the flowers gradually start to wither,
261 and decrease of terpenoids and benzenoid alcohols VOCs emission is observed. However, starting
262 from 05:00 (Stage 11), esters again constituted the majority of VOCs till the flower fully withers
263 (Fig. 1g). Interestingly, both trans-Geraniol and benzyl alcohol displayed a single-peak emission
264 pattern, while methyl salicylate exhibited unusual two peaks (Fig. 1g), indicating the potential

265 competition for substrate allocation within the benzenoid biosynthesis pathway.

266 **3.2 The floral scent is mainly emitted from petal and sepal of *E. oxypetalum***

267 To locate the predominant site for floral VOC biosynthesis and emission, we analyzed
268 volatile profiles of five organs, namely petal, sepal, floral tube, stamen and pistil (Fig. 2a) at three
269 flower developmental stages: pre-Bloom (S1), Blooming (S8) and post-Bloom (S13) using solid
270 phase micro-extraction. In total, 92, 105, 77, 82 and 72 peaks were detected in respective tissue
271 samples. Composition of almost all tissues at pre-Bloom and post-Bloom, as well as Blooming
272 stages of stamens and perianth tubes showed high similarity; Sepals and petals at Blooming
273 clustered away from pre-/post-Bloom samples, while pistils at Blooming grouped separately (Fig.
274 2b). Indeed, At Blooming stage, Both Petal and Sepal samples showed higher trans-Geraniol (Fig.
275 2c) and Benzyl alcohol (Fig. 2d) dry-weight based content than perianth tube and stamen.
276 interestingly, pistil showed excessively high Methyl salicylate content unseen in all other tissues
277 (Fig 2e). However, due to pistil's tiny contribution total flower (Fig. 2f), its contribution to total
278 VOCs emission is considerably small (Fig. 2g). All tested samples showed abundant small fatty
279 acid derivatives, mostly hexanal, which is indicator for tissue damage caused by freezing (Fig. 2g).
280 Therefore, our results identified Petal and Sepal as major VOCs emission site during *E.*
281 *oxypetalum* blooming.

282 **3.3 A cytosol-localized subfamily-a terpene synthase is responsible for trans-Geraniol**
283 **biosynthesis**

284 Since trans-Geraniol was found to be the most dominant component of *E. oxypetalum* floral
285 scent, our subsequent analyses focused on its biosynthesis. A total of 242.13 million reads were
286 generated from 9 libraries, resulting in the assembly of 164,996 unigenes and 299,340 transcripts.
287 The average contig N50 was 2,339 bp. During the BLAST analysis with the sprot and nr database,
288 we found that 64.20% of the transcripts were annotated. Additionally, 45.52% of the transcripts
289 were tagged by GO with an E-value threshold of 1e-5 for all BLAST operations. TMM values
290 were utilized for gene expression quantification.

291 To identify the terpene synthases (TPS) responsible for trans-Geraniol biosynthesis, we
292 extracted transcripts annotated with Pfam TPS models (PF01397.2, PF03936.19, PF19083.3) A

293 total of 84 nonredundant peptides from 23 unigenes were identified as putative TPSs, with eight of
294 them were detected with the significant high expression (Fig. 3a). Sequence clustering analysis on
295 these 23 putative TPSs from *E. oxypetalum* and 342 TPS sequences from 9 other species yield 7
296 subfamilies, with 17 *E. oxypetalum* TPSs belonging to subfamily-a, 1 TPS to subfamily-b, 1 to
297 subfamily-c, 1 to subfamily-e and 3 to subfamily-g (Fig. 3c). Out of all the putative TPSs
298 identified, the transcript *DN1377.2.1.2* from subfamily-a exhibited significantly higher expression
299 levels. Compared to both the pre-Bloom and post-Bloom stages, this particular transcript,
300 designated as *eoTPSa1*, exhibited approximately a 63-fold up-regulation during the Blooming
301 stage, coincided with the peak emission of trans-Geraniol during full bloom.

302 The predicted protein sequence of *eoTPSa1* has an Open Reading Frame (ORF) of 1638 bp,
303 resulting in a protein with 545 amino acids and a molecular weight of 63.29 kDa. Alignment of
304 this protein with other functionally validated geraniol synthase (GES) revealed the presence of
305 conserved Aspartate-rich DDxxD and NSE/DTE motifs, which are important for the
306 magnesium-dependent prenyl diphosphate ionization in class-I mechanisms for terpene synthases.
307 Additionally, a DxDD-like motif, commonly observed in class-II terpene synthases, was also
308 identified (Fig. 3d). Protein structure prediction indicated the characteristic α-β domain structure
309 of monoterpene synthases. The amino acid residue Asp^{294}, Asp^{298}, Asn^{440} and Glu^{448} are in the
310 correct conformation for the binding of magnesium ions (Fig. 3b). The alpha helixes in the α
311 domain form a porous pocket for substrate binding and enable water quenching of carbon cation
312 intermediates for trans-Geraniol formation. The validity of this structure was confirmed through
313 molecular docking simulations. The catalytic ability of *EoTPSa1* has been verified through an *in*
314 *vitro* enzymatic assay using geraniol pyrophosphate as the substrate (Fig. 4).

315 Additionally, *EoTPSa1* is predicted to be localized in the cytosol, alongside the highly
316 expressed geranyl pyrophosphate synthase in *E. oxypetalum*, namely *EoGDPS*. This finding
317 distinguishes *EoTPSa1* from other characterized geraniol synthases that are typically transported
318 into plastids. We further validated the cytosol localization of *EoTPSa1* and *EoGDPS* through
319 *Nicotiana* transient expression system. We detected strong GFP signals in the cytosols of
320 transformed leaf epidermis for all *EoTPSa1*-GFP, *EoGDPS*-GFP and pure GFP constructs,
321 suggesting an absence of N-terminus transport peptide activity (Fig. 5). These results posed a

322 special cytosol localized geraniol synthase unseen in previous literature, indicating an uncanonical
323 cytosol-localized monoterpene synthesis route for monoterpene in the night blooming *E.*
324 *oxypetalum* flowers.

325 **3.4 MVA pathway mainly provides precursors for trans-Geraniol biosynthesis**

326 Next, to validate this cytosol-localized monoterpene biosynthesis, we investigated the
327 biosynthetic origin of trans-Geraniol precursors, namely IPP and DMAPP. Indeed, homologous
328 genes from the MVA pathway experienced upregulation at blooming stage, contrary to the
329 uniformly low expression of MEP pathway genes across all three time points. The *HMG* gene,
330 which encodes a putative hydroxymethylglutaryl-CoA reductase and acts as the rate-limiting
331 enzyme of MVA pathway, experienced a 69-fold upregulation at Blooming stage compared to the
332 pre-Bloom stage (TMM 35.89 vs 2463.66). Another gene, *MVAD*, which encodes a putative
333 diphosphate-mevalonate decarboxylase, also exhibited a two-fold upregulation (Fig. 6a). Next, we
334 blocked the MVA and MEP pathways with specific inhibitors: mevinolin for MVA and
335 fosmidomycin for MEP, respectively. Interestingly, Mevinolin treated flowers clustered
336 independent of both Fosmidomycin-treated and control group (Fig. 6b, c). indeed, the major scent
337 volatile trans-Geraniol decreased by an average of 83.38%, comparing mevinolin-treated to
338 control groups. In contrast, fosmidomycin-treated flowers showed a slight increase of 8.44% in
339 trans-Geraniol emission, possibly due to the blockage of metabolic flow intended for
340 sesquiterpene production (Fig. 6d). Shift of volatile composition toward a benzenoid-dominated
341 blend is observed, indicating disrupted metabolic flow caused by mevinolin's inhibition of *HMG*
342 and carbon flow towards benzenoid biosynthesis pathways (Fig. 6f). Collectively, these findings
343 demonstrate that the MVA pathway is a major, if not the sole, contributor of IPP and DMAPP for
344 trans-Geraniol biosynthesis. Also, these results confirm the presence of an uncanonical
345 cytosol-localized geraniol synthase in the night blooming of *E. oxypetalum.*

346 **3.5 Amyloplast provides carbon source for floral VOCs biosynthesis**

347 To investigate the biological sources of trans-Geraniol synthesis catalyzed by the MVA
348 pathway in *E. oxypetalum*, expression pattern of homologous genes from starch degradation,
349 glycolysis along with triglyceride degradation and β-oxidation were determined (Fig. 7a).

350 Generally, the identified genes showed higher, if not constant expression at pre-Bloom stage than
351 Blooming and post-Bloom stage. The beta amylase *BAM*, which catalyzes initial step of starch
352 degradation, showed 6.8 times upregulation at full-Bloom. This is in concord with the constant
353 decreased starch (Fig. 7b) and elevated reducing sugar (Fig. 7c) and pyruvate (Fig. 7d) content
354 detected in petal before blooming. in great contrast, both triglyceride and free fatty acid showed
355 almost undetectable content, while accumulated acetyl-CoA (Fig. 7e), the direct substrate for
356 MVA pathway, were gradually used up by the active metabolism at the day of flowering. TEM
357 images also suggest disappeared amyloplast at Blooming (Fig. 8). Together, our results suggest
358 starch granule from amyloplast provides carbon source for floral VOCs.

359 # 4. Discussion

360 ## 4.1 Explosive floral VOCs emission functions in pollinator adaption

361 Composition of plant volatiles is highly dynamic and context dependent, especially for active
362 physiological processes such as flowering and stress response (Farre-Armengol *et al.*, 2013).
363 Floral VOCs emission generally coincides with flower opening. For slow-blooming flowers such
364 as rose and petunia that last for several days (Oyama-Okubo *et al.*, 2005), circadian oscillation is
365 commonly observed (Fenske & Imaizumi, 2016). An interesting case of *Lonicera japonica*
366 (Caprifoliaceae) flower, which blooms twice during two consecutive days, reaches emission peak
367 with different VOC composition at each blooming (Feng *et al.*). These variations are greatly
368 results of different pollination strategies and adaptation to local environments.

369 Strong scent and impressive flowers are widely distributed across Cactaceae (Kaiser &
370 Tollsten, 1995). This family can be recognized by very fleshy stems and fruits, both adaptive traits
371 to the ancestral succulent biome. Its adaptation to dry conditions probably first evolved in the
372 central Andeans (Hernández-Hernández *et al.*, 2014), and subsequently diversified into numerous
373 biomes across the Americas and some part of Asia and Africa (Barthlott *et al.*, 2015). The *E.*
374 *oxypetalum* flowers, which are native to central America jungles, has broad leaf-like stems with
375 huge white flowers. The night blooming and explosive scent emission maybe a legacy of drought
376 adaptation, where scorching sun during the day discourage pollinator activity and easily destroy
377 soft floral tissue without cuticle wax protection (Wang *et al.*, 2020).

378 Cactaceae flowers evolved hypanthium, long floral tube and diverse floral scent as key
379 innovations, allowing greater pollinator diversity (Patiny, 2012). The scent of nocturnal Cacti
380 flowers reaches two extremes, with moth-pollinating flowers emits delighting terpene- or
381 aromatics- rich aromas, and bat-pollinating flowers emits sulfur-containing leek-like odor. These
382 nocturnal flowers generally are white or greenish, and open during one night only (Kaiser &
383 Tollsten, 1995). Bee pollination is probably plesiomorphic for Cactaceae species, while several
384 bee-to-moth or -bird shifts have been proposed especially in Cactoideae (Patiny, 2012).
385 Hawkmoth adores the pleasing aroma of terpenoids VOCs, such as linalool (Miyake *et al.*, 1998)
386 or trans-Geraniol of *E. oxypetalum*. These evidences provides yet another case for possible

387 co-evolution between nocturnal cacti and its moth pollinators using specific volatiles as identifier.

388 **4.2 Cytosolic trans-Geraniol synthesis shows metabolism plasticity**

389 The MEP pathway is commonly believed to provide C_5 precursors for monoterpene volatile
390 biosynthesis (Piel *et al.*, 1998; Dudareva *et al.*, 2005). Together with plastid-localized GPP
391 synthase and geraniol synthase (Simkin *et al.*, 2013), plastid are thought as the canonical synthesis
392 hub for monoterpene VOCs of various species and tissues (Schuhr *et al.*, 2003). Previous transient
393 expression experiments suggest geraniol biosynthesis capacity of different subcellular
394 compartments is influenced by local geranyl diphosphate availability (Dong *et al.*, 2016).
395 Correspondingly, almost all characterized geraniol synthases in TPS family are plastid localized
396 (Chen *et al.*, 2016; Abbas *et al.*, 2019; Zhao *et al.*, 2020), except for one from *Lippia dulcis*
397 located in both cytosol and plastid, which is proved with reduced activity in *Nicotiana* system
398 (Dong, 2013). Though metabolic crosstalk also exists between MVA and MEP pathways (Koley *et*
399 *al.*, 2020), MEP pathway usually takes central stage for monoterpene biosynthesis under most
400 scenarios.

401 However, in *E. oxypetalum* petal, our results showed clear MVA dominance and cytosolic
402 localization of monoterpene volatiles biosynthesis in petal. Both transcriptomic evidence and
403 pathway inhibitor assay proved MVA pathway provides most direct precursors for monoterpene
404 biosynthesis, while the unique cytosol-localized *EoTPSa1* is identified as the gene responsible for
405 the predominant monoterpene volatile trans-Geraniol biosynthesis. The dramatic strong VOCs
406 emission indicates high local GPP content and high synthase activity. interestingly, unlike geraniol
407 synthases identified in other species, the biochemically validated *E. oxypetalum* geraniol synthase
408 is clustered into TPS-a clade. Previous study divided the TPS family into 7 subfamilies from
409 TPS-a to TPS-h, each with different presumed function (Chen *et al.*, 2011). Generally, subfamily-a
410 TPSs are generally thought to catalyse sesquiterpene formation in cytosol. This unusual clustering
411 suggests possible sequence deletion and possible neofunctionalization event during its
412 evolutionary history.

413 **4.3 Subcellular structure might participate in the explosive scent emission**

414 Volatile production is usually linked with certain cells or compartments like secretory cells or

resin ducts (Ghissing & Mitra, 2020). However, these specialized tissue-scale cavities were not observed in *E. oxypetalum* petal. On the other hand, besides the disappeared amyloplast that function as carbon source during flowering, an unexpected irregular oval body is discovered in TEM images (Fig. 8). We first suspected this oval shape as lipid body, the storage subcellular structure that were usually observed in seeds, to work synchronously with amyloplast in providing carbon source and reducing power for volatile synthesis. However, electron density and quantification of triglyceride dictates otherwise. The greater electron density and greyish appearance under TEM is similar to protein bodies, a membrane-bound structure which stores protein for further use. This unknown structure might hold answers to the explosive volatile emission, as sudden release of stored enzymes can initiate metabolism all of sudden. Unfortunately, since no specific staining protocol is viable for protein body, and no transformation protocol has been developed for *E. oxypetalum* plants for fusion protein *in vivo* expression. The exploration for the functionality of this unknown structure will be our next task.

Acknowledgements

We further wish to thank Jie Yu and Ying Hao for completing the cryoelectron microscopy experiment; Yudong Ma, Wei Wu and Jin Dai for their assistance in sample collection; Bolei Jiao, Xinrui Liu and Chuanfang Wu for sharing the *N. benthamiana* plants and pSuper1300, pET-28a plastids.

Competing interests

None declared

Author contributions

Yiyang Zhang, Yuhan Zhang, LT and QS designed the experiments. Yiyang Zhang and Yuhan Zhang quantified VOCs content with GCMS. YiYang Zhang analyzed GCMS and transcriptome data. Yuhan Zhang and QT performed molecular cloning, enzymatic assay and localization studies. LW performed biochemical quantifications. Yiyang Zhang plot the figures and wrote the manuscript. Yuhan Zhang, QS, TL and HX revised the manuscript. WT provided germplasm used in the current study. Yiyang Zhang and Yuhan Zhang contributed equally to this work.

Data Availability

We will upload the sequence information after receiving the article.

447 ## References

448 **Abbas F, Ke Y, Yu R, Fan Y**. **2019**. Functional characterization and expression analysis of two
449 terpene synthases involved in floral scent formation in Lilium 'Siberia'. *Planta* **249**: 71–93.

450 **Abbas F, Ke Y, Yu R, Yue Y, Amanullah S, Jahangir MM, Fan Y**. **2017**. Volatile terpenoids: multiple
451 functions, biosynthesis, modulation and manipulation by genetic engineering. *Planta* **246**:
452 803–816.

453 **Altschul SF, Gish W, Miller W, Myers EW, Lipman DJ**. **1990**. Basic local alignment search tool.
454 *Journal of Molecular Biology* **215**: 403–410.

455 **Barthlott W, Burstedde K, Geffert JL**. **2015**. *Biogeography and Biodiversity of Cacti*.

456 **Bolger AM, Lohse M, Usadel B**. **2014**. Trimmomatic: a flexible trimmer for Illumina sequence
457 data. *Bioinformatics* **30**: 2114–2120.

458 **Chang T-H, Guo R-T, Ko T-P, Wang AH-J, Liang P-H**. **2006**. Crystal Structure of Type-III
459 Geranylgeranyl Pyrophosphate Synthase from Saccharomyces cerevisiae and the Mechanism of
460 Product Chain Length Determination. *Journal of Biological Chemistry* **281**: 14991–15000.

461 **Chen F, Li W, Jiang L, Pu X, Yang Y, Zhang G, Luo Y**. **2016**. Functional characterization of a geraniol
462 synthase-encoding gene from Camptotheca acuminata and its application in production of
463 geraniol in Escherichia coli. *Journal of Industrial Microbiology & Biotechnology* **43**: 1281–1292.

464 **Chen F, Tholl D, Bohlmann J, Pichersky E**. **2011**. The family of terpene synthases in plants: a
465 mid-size family of genes for specialized metabolism that is highly diversified throughout the
466 kingdom: Terpene synthase family. *The Plant Journal* **66**: 212–229.

467 **Chen W, Viljoen AM**. **2010**. Geraniol — A review of a commercially important fragrance material.
468 *South African Journal of Botany* **76**: 643–651.

469 **Christianson DW**. **2017**. Structural and Chemical Biology of Terpenoid Cyclases. *Chemical Reviews*
470 **117**: 11570–11648.

471 **Darriba D, Posada D, Kozlov AM, Stamatakis A, Morel B, Flouri T**. **2020**. ModelTest-NG: A New
472 and Scalable Tool for the Selection of DNA and Protein Evolutionary Models. *Molecular Biology*
473 *and Evolution* **37**: 291–294.

474 **Dodson C, Hills H**. **1966**. Gas Chromatography of Orchid Fragrances. *Studies in Orchid Pollination*:
475 720–721.

476 **Dong L**. **2013**. Characterization of two geraniol synthases from Valeriana officinalis and Lippia
477 dulcis_ Similar activity but difference in subcellular localization. *Metabolic Engineering*.

478 **Dong L, Jongedijk E, Bouwmeester H, Van Der Krol A**. **2016**. Monoterpene biosynthesis potential
479 of plant subcellular compartments. *New Phytologist* **209**: 679–690.

480 **Duarte GT, Volkova PYu, Geras'kin SA**. **2021**. A Pipeline for Non-model Organisms for de novo
481 Transcriptome Assembly, Annotation, and Gene Ontology Analysis Using Open Tools: Case Study
482 with Scots Pine. *Bio-protocol* **11**: e3912.

483 **Dudareva N, Andersson S, Orlova I, Gatto N, Reichelt M, Rhodes D, Boland W, Gershenzon J**.
484 **2005**. The nonmevalonate pathway supports both monoterpene and sesquiterpene formation in
485 snapdragon flowers. *Proceedings of the National Academy of Sciences* **102**: 933–938.

486 **Dudareva N, Klempien A, Muhlemann JK, Kaplan I**. **2013**. Biosynthesis, function and metabolic
487 engineering of plant volatile organic compounds. *New Phytologist* **198**: 16–32.

488 **Dynamic pathway allocation in early terpenoid biosynthesis of stress-induced lima bean leaves**.
489 **2006**. *Phytochemistry* **67**: 1661–1672.

490 **Eddy SR**. **2011**. Accelerated Profile HMM Searches (WR Pearson, Ed.). *PLoS Computational*
491 *Biology* **7**: e1002195.

492 **Edgar RC**. **2004**. MUSCLE: multiple sequence alignment with high accuracy and high throughput.
493 *Nucleic Acids Research* **32**: 1792–1797.

494 **Eltz T, Roubik DW, Lunau K**. **2005**. Experience-dependent choices ensure species-specific
495 fragrance accumulation in male orchid bees. *Behavioral Ecology and Sociobiology* **59**: 149–156.

496 **Farre-Armengol G, Filella I, Llusia J, Penuelas J**. **2013**. Floral volatile organic compounds:
497 Between attraction and deterrence of visitors under global change. *Perspectives in Plant Ecology*
498 *Evolution and Systematics* **15**: 56–67.

499 **Feng H-H, Wang X-Y, Luo Y-B, Huang S-Q**. Floral scent emission is the highest at the second night
500 of anthesis in Lonicera japonica (Caprifoliaceae). *Journal of Systematics and Evolution* **n/a**.

501 **Fenske MP, Imaizumi T**. **2016**. Circadian Rhythms in Floral Scent Emission. *Frontiers in Plant*
502 *Science* **7**.

503 **Ghissing U, Mitra A**. **2020**. Biology of Floral Scent Volatiles in Ornamental Plants. In: Datta SK,
504 Gupta YC, eds. Handbooks of Crop Diversity: Conservation and Use of Plant Genetic Resources.
505 Floriculture and Ornamental Plants. Singapore: Springer, 1–41.

506 **Grabherr MG, Haas BJ, Yassour M, Levin JZ, Thompson DA, Amit I, Adiconis X, Fan L,**
507 **Raychowdhury R, Zeng Q, *et al.* 2011**. Trinity: reconstructing a full-length transcriptome without
508 a genome from RNA-Seq data. *Nature biotechnology* **29**: 644–652.

509 **Gutensohn M, Orlova I, Nguyen TTH, Davidovich-Rikanati R, Ferruzzi MG, Sitrit Y, Lewinsohn E,**
510 **Pichersky E, Dudareva N**. **2013**. Cytosolic monoterpene biosynthesis is supported by
511 plastid-generated geranyl diphosphate substrate in transgenic tomato fruits. *The Plant Journal* **75**:
512 351–363.

513 **Haas BJ, Papanicolaou A, Yassour M, Grabherr M, Blood PD, Bowden J, Couger MB, Eccles D, Li**

514 **B, Lieber M, *et al.* 2013**. De novo transcript sequence reconstruction from RNA-Seq: reference
515 generation and analysis with Trinity. *Nature protocols* **8**: 10.1038/nprot.2013.084.

516 **Heiling AM**. **2004**. Exploitation of floral signals by crab spiders (Thomisus spectabilis, Thomisidae).
517 *Behavioral Ecology* **15**: 321–326.

518 **Hernández-Hernández T, Brown JW, Schlumpberger BO, Eguiarte LE, Magallón S**. **2014**. Beyond
519 aridification: multiple explanations for the elevated diversification of cacti in the New World
520 Succulent Biome. *New Phytologist* **202**: 1382–1397.

521 **Jumper J, Evans R, Pritzel A, Green T, Figurnov M, Ronneberger O, Tunyasuvunakool K, Bates R,**
522 **Žídek A, Potapenko A, *et al.* 2021**. Highly accurate protein structure prediction with AlphaFold.
523 *Nature* **596**: 583–589.

524 **Kaiser R, Tollsten L**. **1995**. An introduction to the scent of cacti. *Flavour and Fragrance Journal* **10**:
525 153–164.

526 **Kanehisa M, Goto S**. **2000**. KEGG: Kyoto Encyclopedia of Genes and Genomes. *Nucleic Acids*
527 *Research* **28**: 27–30.

528 **Kita T, Brown MS, Goldstein JL**. **1980**. Feedback regulation of 3-hydroxy-3-methylglutaryl
529 coenzyme A reductase in livers of mice treated with mevinolin, a competitive inhibitor of the
530 reductase. *The Journal of Clinical Investigation* **66**: 1094–1100.

531 **Knudsen JT, Eriksson R, Gershenzon J**. Diversity and Distribution of Floral Scent. *THE BOTANICAL*
532 *REVIEW*.

533 **Koley S, Grafahrend-Belau E, Raorane ML, Junker BH**. **2020**. *The mevalonate pathway*
534 *contributes to monoterpene production in peppermint*. Plant Biology.

535 **Kozlov AM, Darriba D, Flouri T, Morel B, Stamatakis A**. **2019**. RAxML-NG: a fast, scalable and
536 user-friendly tool for maximum likelihood phylogenetic inference. *Bioinformatics* **35**: 4453–4455.

537 **Letunic I, Bork P**. **2021**. Interactive Tree Of Life (iTOL) v5: an online tool for phylogenetic tree
538 display and annotation. *Nucleic Acids Research* **49**: W293–W296.

539 **Li B, Dewey CN**. **2011**. RSEM: accurate transcript quantification from RNA-Seq data with or
540 without a reference genome. *BMC bioinformatics* **12**: 323.

541 **Love MI, Huber W, Anders S**. **2014**. Moderated estimation of fold change and dispersion for
542 RNA-seq data with DESeq2. *Genome Biology* **15**: 550.

543 **Mendoza-Poudereux I, Kutzner E, Huber C, Segura J, Eisenreich W, Arrillaga I**. **2015**. Metabolic
544 cross-talk between pathways of terpenoid backbone biosynthesis in spike lavender. *Plant*
545 *Physiology and Biochemistry* **95**: 113–120.

546 **Mistry J, Chuguransky S, Williams L, Qureshi M, Salazar GA, Sonnhammer ELL, Tosatto SCE,**
547 **Paladin L, Raj S, Richardson LJ, *et al.* 2021**. Pfam: The protein families database in 2021. *Nucleic*

548 *Acids Research* **49**: D412–D419.

549 **Miyake T, Yamaoka R, Yahara T**. **1998**. Floral scents of hawkmoth-pollinate flowers in Japan.
550 *Journal of Plant Research* **111**: 199–205.

551 **Morris GM, Huey R, Lindstrom W, Sanner MF, Belew RK, Goodsell DS, Olson AJ**. **2009**.
552 AutoDock4 and AutoDockTools4: Automated Docking with Selective Receptor Flexibility. *Journal*
553 *of computational chemistry* **30**: 2785–2791.

554 **Muhlemann JK, Klempien A, Dudareva N**. **2014**. Floral volatiles: from biosynthesis to function.
555 *Plant Cell and Environment* **37**: 1936–1949.

556 **Opitz S, Nes WD, Gershenzon J**. **2014**. Both methylerythritol phosphate and mevalonate
557 pathways contribute to biosynthesis of each of the major isoprenoid classes in young cotton
558 seedlings. *Phytochemistry* **98**: 110–119.

559 **Oyama-Okubo N, Ando T, Watanabe N, Marchesi E, Uchida K, Nakayama M**. **2005**. Emission
560 mechanism of floral scent in Petunia axillaris. *Bioscience, Biotechnology, and Biochemistry* **69**:
561 773–777.

562 **Parachnowitsch AL, Raguso RA, Kessler A**. **2012**. Phenotypic selection to increase floral scent
563 emission, but not flower size or colour in bee-pollinated Penstemon digitalis. *New Phytologist* **195**:
564 667–675.

565 **Patiny S (Ed.)**. **2012**. *Evolution of plant-pollinator relationships*. Cambridge ; New York: Cambridge
566 University Press.

567 **Piel J, Donath J, Bandemer K, Boland W**. **1998**. Mevalonate-Independent Biosynthesis of
568 Terpenoid Volatiles in Plants: Induced and Constitutive Emission of Volatiles. *Angewandte Chemie*
569 *(International Ed. in English)* **37**: 2478–2481.

570 **Qiao Z, Hu H, Shi S, Yuan X, Yan B, Chen L**. **2021**. An Update on the Function, Biosynthesis and
571 Regulation of Floral Volatile Terpenoids. *Horticulturae* **7**: 451.

572 **Quintanilla-Casas B, Bro R, Hinrich JL, Davie-Martin CL**. **2023**. *Tutorial on PARADISe:*
573 *PARAFAC2-based Deconvolution and Identification System for processing GC–MS data*. Protocol
574 Exchange.

575 **Raguso RA**. **2008**. Wake Up and Smell the Roses: The Ecology and Evolution of Floral Scent.
576 *Annual Review of Ecology, Evolution, and Systematics* **39**: 549–569.

577 **Sachse S, Galizia CG**. **2003**. The coding of odour-intensity in the honeybee antennal lobe: local
578 computation optimizes odour representation. *The European Journal of Neuroscience* **18**:
579 2119–2132.

580 **Schuhr CA, Radykewicz T, Sagner S, Latzel C, Zenk MH, Arigoni D, Bacher A, Rohdich F,**
581 **Eisenreich W**. **2003**. Quantitative assessment of crosstalk between the two isoprenoid

582 biosynthesis pathways in plants by NMR spectroscopy. *Phytochemistry Reviews* **2**: 3–16.

583 **Simkin AJ, Miettinen K, Claudel P, Burlat V, Guirimand G, Courdavault V, Papon N, Meyer S,**
584 **Godet S, St-Pierre B, *et al.* 2013**. Characterization of the plastidial geraniol synthase from
585 Madagascar periwinkle which initiates the monoterpenoid branch of the alkaloid pathway in
586 internal phloem associated parenchyma. *Phytochemistry* **85**: 36–43.

587 **Tan KH, Nishida R**. **2007**. Zingerone in the floral synomone of Bulbophyllum baileyi (Orchidaceae)
588 attracts Bactrocera fruit flies during pollination. *Biochemical Systematics and Ecology* **35**:
589 334–341.

590 **The Gene Ontology Consortium, Aleksander SA, Balhoff J, Carbon S, Cherry JM, Drabkin HJ,**
591 **Ebert D, Feuermann M, Gaudet P, Harris NL, *et al.* 2023**. The Gene Ontology knowledgebase in
592 2023. *Genetics* **224**: iyad031.

593 **Wang X, Kong L, Zhi P, Chang C**. **2020**. Update on Cuticular Wax Biosynthesis and Its Roles in Plant
594 Disease Resistance. *International Journal of Molecular Sciences* **21**: 5514.

595 **Young MD, Wakefield MJ, Smyth GK, Oshlack A**. **2010**. Gene ontology analysis for RNA-seq:
596 accounting for selection bias. *Genome Biology* **11**: R14.

597 **Zhang W, Jiang Y, Chen F, Guan Z, Wei G, Chen X, Zhang C, Köllner TG, Chen S, Chen F, *et al.* 2022**.
598 Dynamic regulation of volatile terpenoid production and emission from Chrysanthemum
599 morifolium capitula. *Plant Physiology and Biochemistry* **182**: 11–21.

600 **Zhao C, Yu Z, Silva JAT da, He C, Wang H, Si C, Zhang M, Zeng D, Duan J**. **2020**. Functional
601 Characterization of a Dendrobium officinale Geraniol Synthase DoGES1 Involved in Floral Scent
602 Formation. *International Journal of Molecular Sciences* **21**: 7005.

603

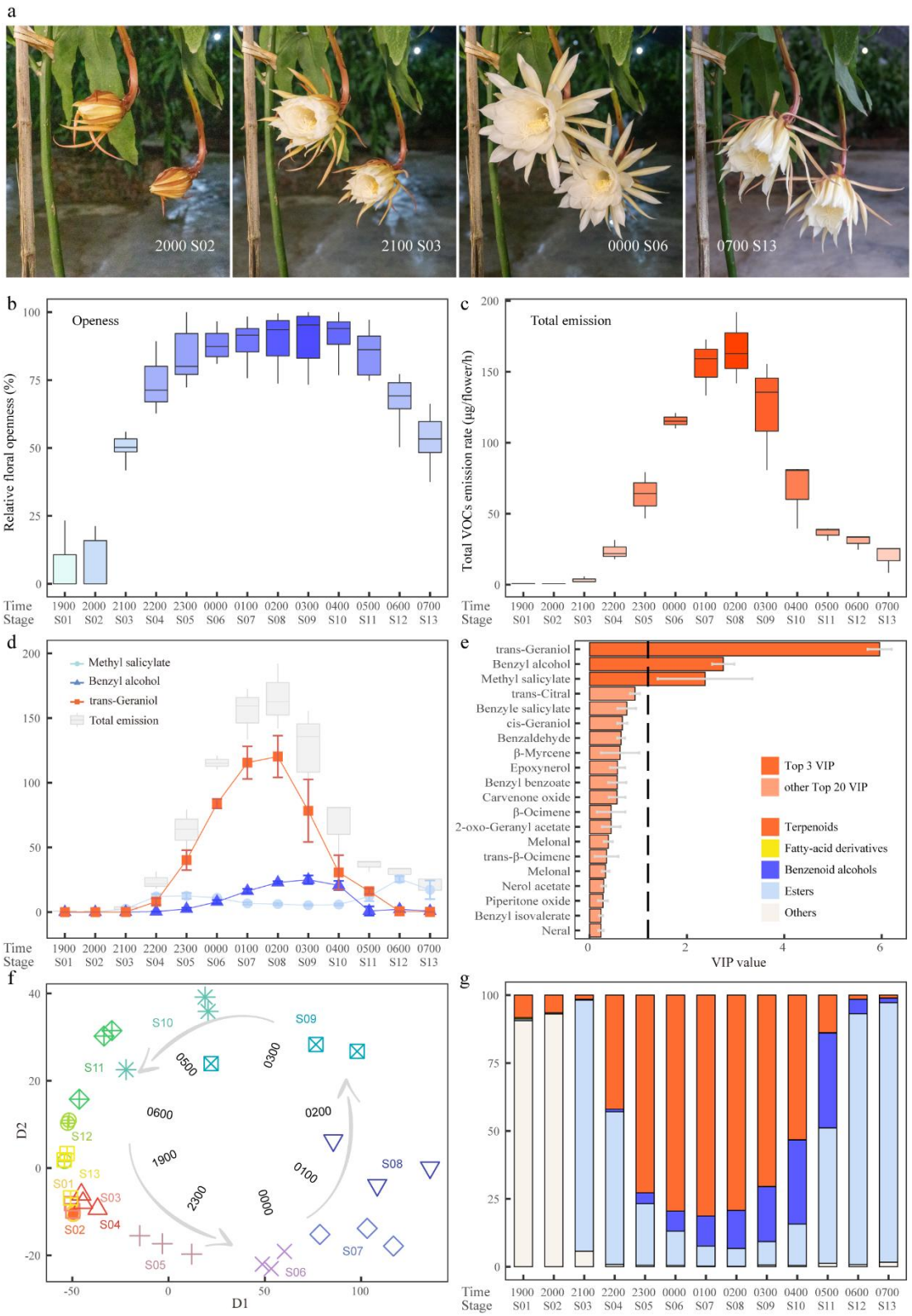

Fig. 1. Temporal patterns of flower opening and volatile organic compounds (VOCs) emission dynamics in *Epiphyllum oxypetalum*

(a): Time-lapse pictures showing rapid flowering of *E. oxypetalum* flower

608 (b): flower openness across the 13 VOC-sampling stages.

609 (c): Emission rate of total floral VOCs across the 13 VOC-sampling stages.

610 (d): VOC emission rate of trans-Geraniol, Benzyl alcohol, Methyl salicylate and total
611 emission across all sampled stages.

612 (e): VIP value of top 20 VOCs from OPLS-DA analysis. The 3 major VOCs with VIP
613 values higher than threshold were colored in brighter red.

614 (f): PCA clustering of floral VOC content. Dots were shaped and colored according to
615 sampling stages, time tags inside arrow rings corresponds to sampling time of nearby
616 dots.

617 (g): Relative concentration of terpenoids, fatty-acid derivatives, benzenoid alcohols,
618 esters and other VOCs across all sampled stages.

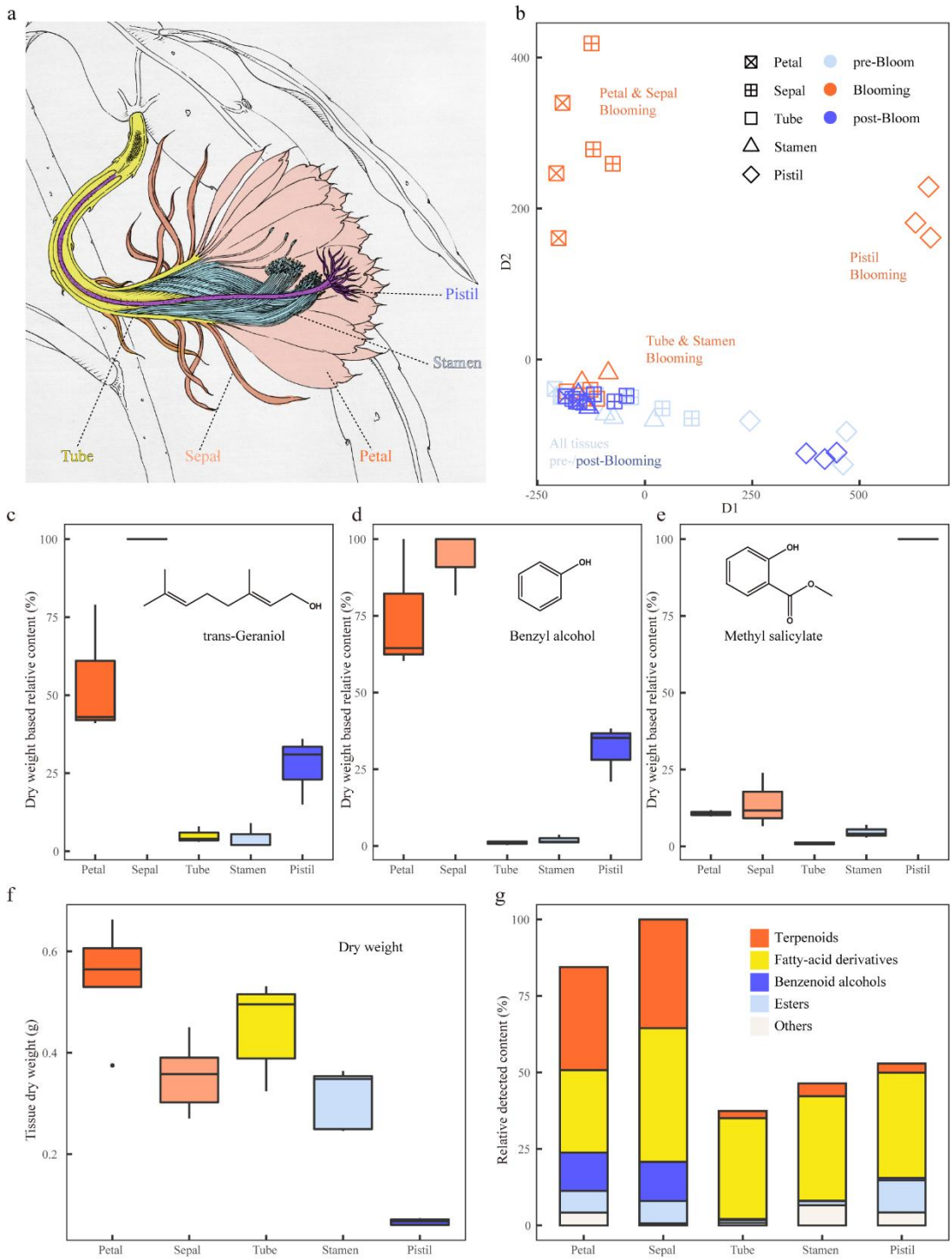

Fig. 2. Emission patterns of five floral tissues at pre-Bloom, Blooming, and post-Bloom

(a): Schematic diagram of *E.oxypetalum* tissue longitudinal section. The 5 sampled tissues are colored differently.

(b): PCA clustering of volatile organic compound (VOC) content of peal, sepal, floral

625 tube, stamen and pistil at pre-Bloom, Blooming and post-Bloom.

626 (c-e): Dry weight based content of trans-Geraniol, Benzyl alcohol and Methyl
627 salicylate of 5 floral tissues at Blooming stage.

628 (f): Dry weight of 5 sampled tissues at Blooming stage.

629 (g): Relative content of 5 major classes VOCs detected at Blooming stage, not
630 adjusted by dry mass.

631

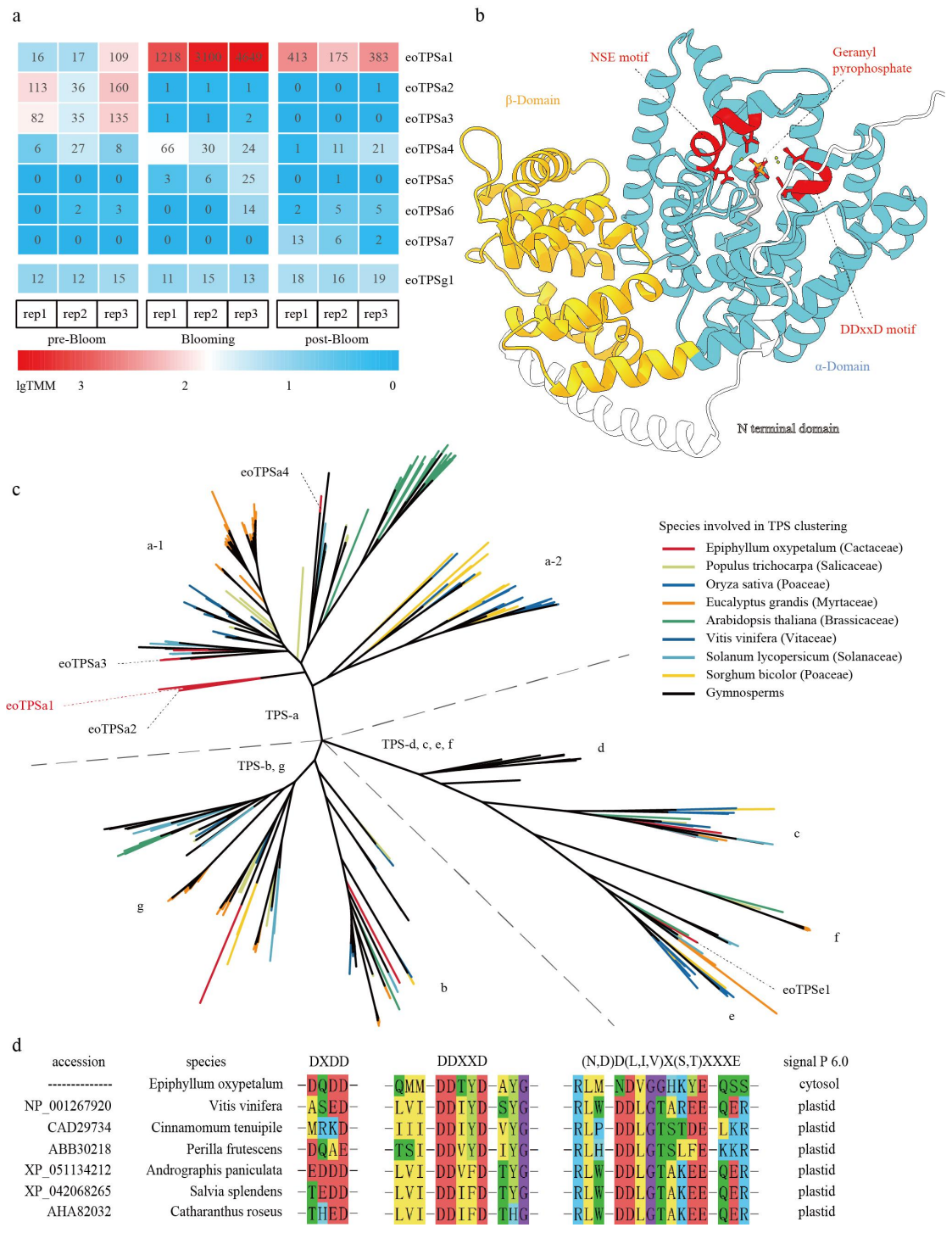

Fig. 3. Identification of the terpene synthase responsible for trans-Geraniol biosynthesis

(a): Expression patterns of 8 terpene synthases identified with significant expression at pre-Bloom, Blooming and post-Bloom, each block is colored according to TMM value.

638 (b): Structure prediction and molecular docking result of EoTPSa1. Protein structure
639 is colored according to domain architecture and catalyzing motifs. Residues of Asp^{294},
640 Asp^{298}, Asn^{440} and Glu^{448} were shown.

641 (c): Clustering of identified *Epiphyllum oxypetalum* TPSs with TPSs from other
642 species. The major TPSs in *E. oxypetalum* petal are marked with dashed line

643 (d) Protein alignment of *EoTPSa1* and GESs from other 6 species, protein sequence
644 around DxDD, DDxxD and NSE/DTE motifs were colored according to amino acid
645 properties. Subcellular localization predicted with signal P 6.0 were also given.

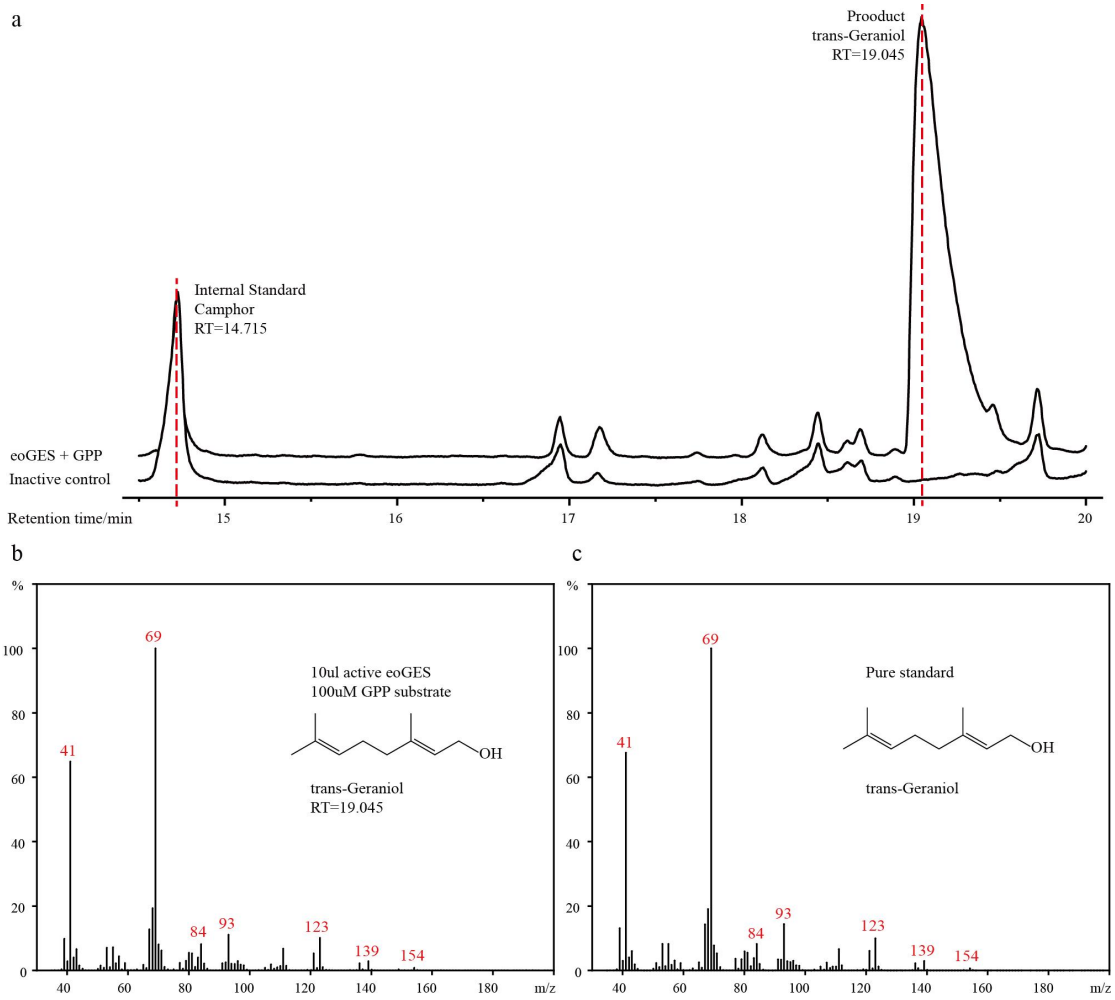

Fig. 4. Biochemical characterization of EoTPSa1 as trans-Geraniol synthase.

(a): TIC comparison between active enzyme and inactive control from 14.5 min to 20min RT, showing huge trans-Geraniol peak at 19.045 RT.

(b): MS detail of trans-Geraniol peak (RT 19.045) catalyzed with *EoTPSa1*.

(c): MS detail of pure trans-Geraniol standard.

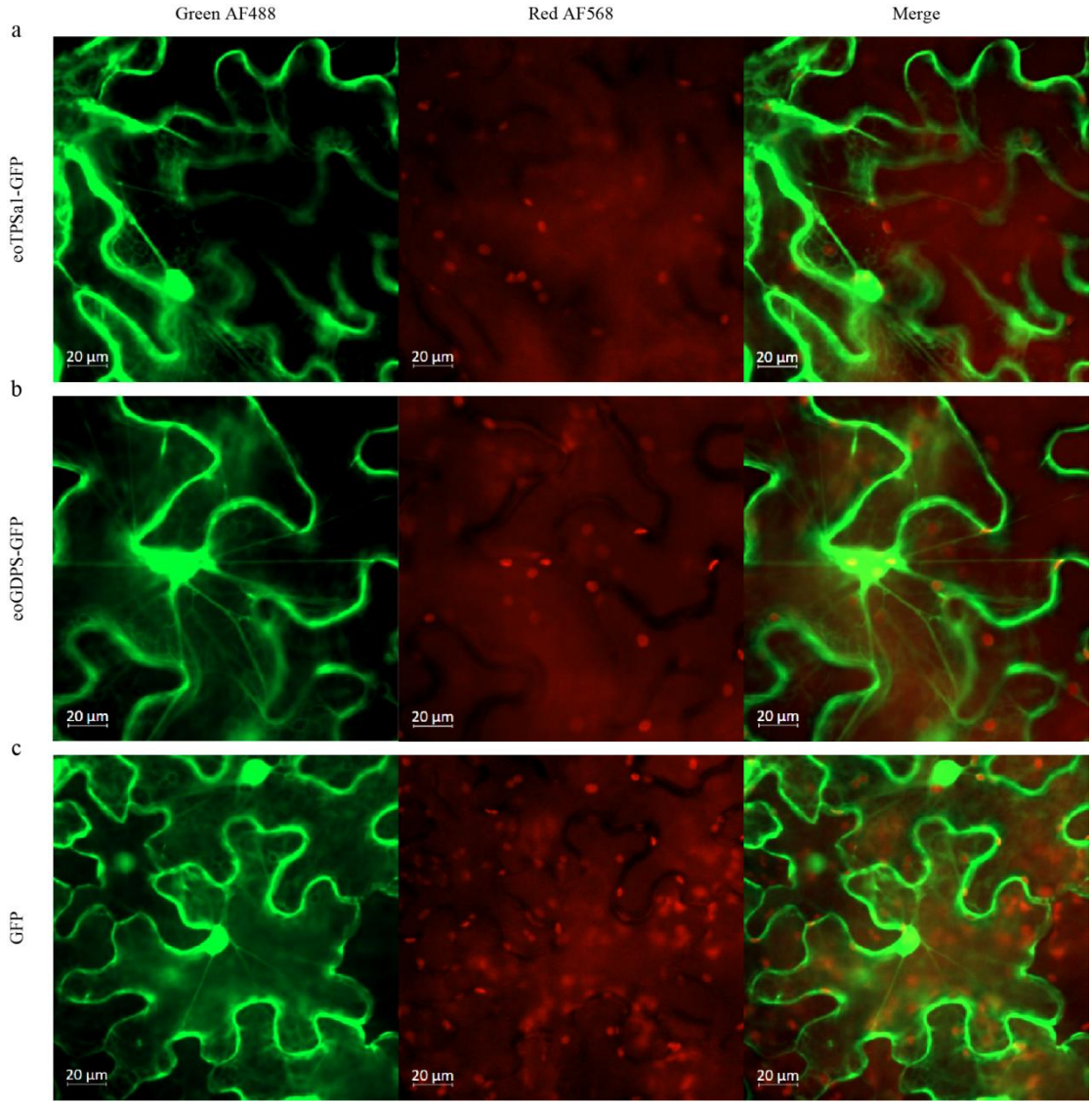

Fig. 5. Subcellular localization of EoTPSa1 and EoGDPS

(a-c): Subcellular localization of EoTPSa1-GFP, EoGDPS-GFP and pure GFP control. Confocal image was taken at AF488 green band to show GFP fluorescence, and AF568 red band to show chloroplast autofluorescence.

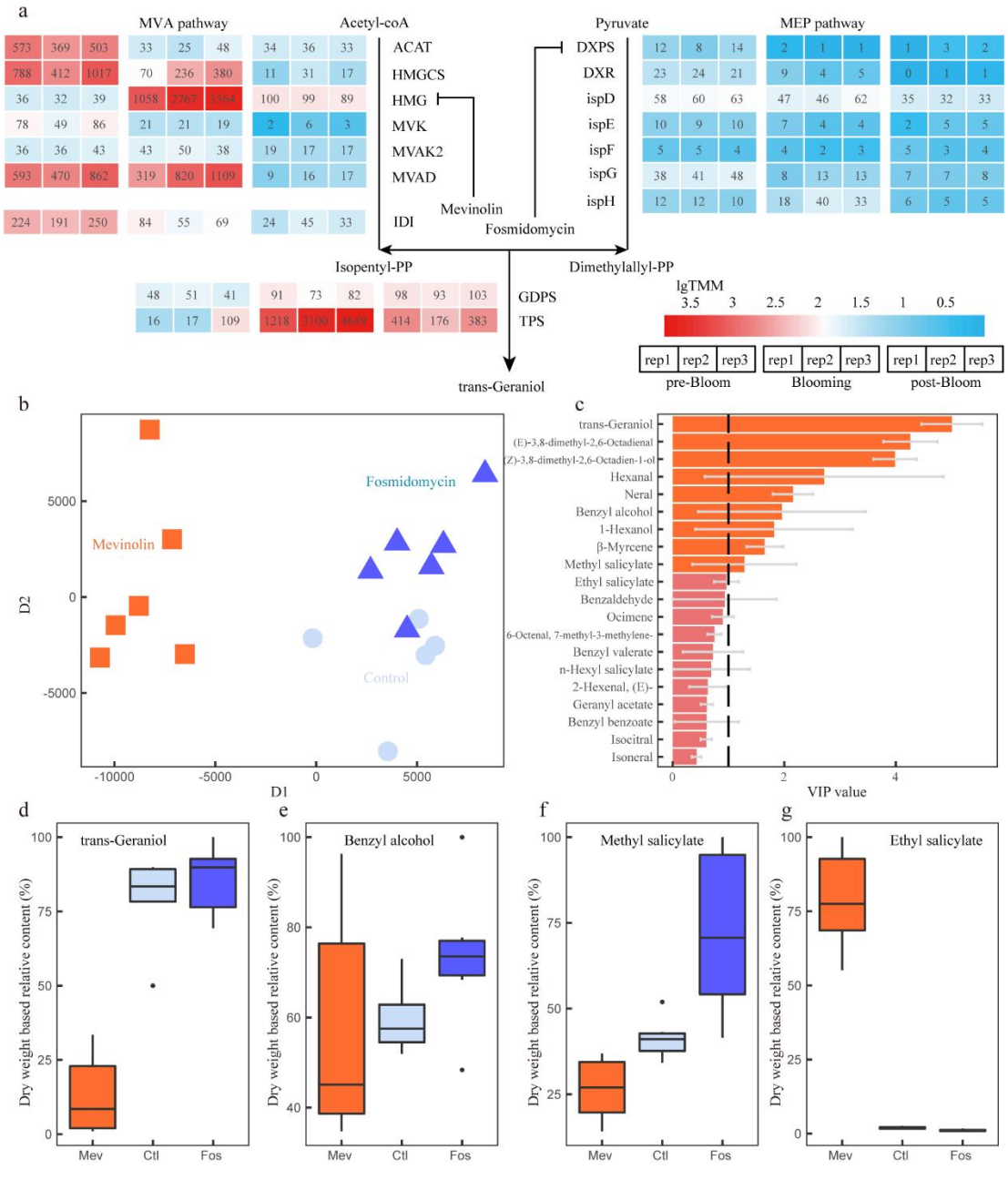

657

658 **Fig. 6. Pathway preference of trans-Geraniol biosynthesis in *Epiphyllum***
659 ***oxypetalum* petal**

660 (a): Expression pattern of MVA and MEP pathway genes at pre-Bloom, Blooming and
661 post-Bloom, each block is colored according to TMM value.

662 (b): PCA clustering of volatile organic compound (VOC) content of petals with
663 mevinolin, fosmidomycin and blank treatment at Blooming. Dots were shaped and
664 colored according different treatments.

665 (c): VIP value of top 20 VOCs from OPLS-DA analysis. VOCs with VIP values
666 higher than threshold were colored in brighter red.

667 (d-g): VOC content of trans-Geraniol, Benzyl alcohol, Methyl salicylate and Ethyl
668 salicylate in petal of mevinolin, fosmidomycin and blank treatment.

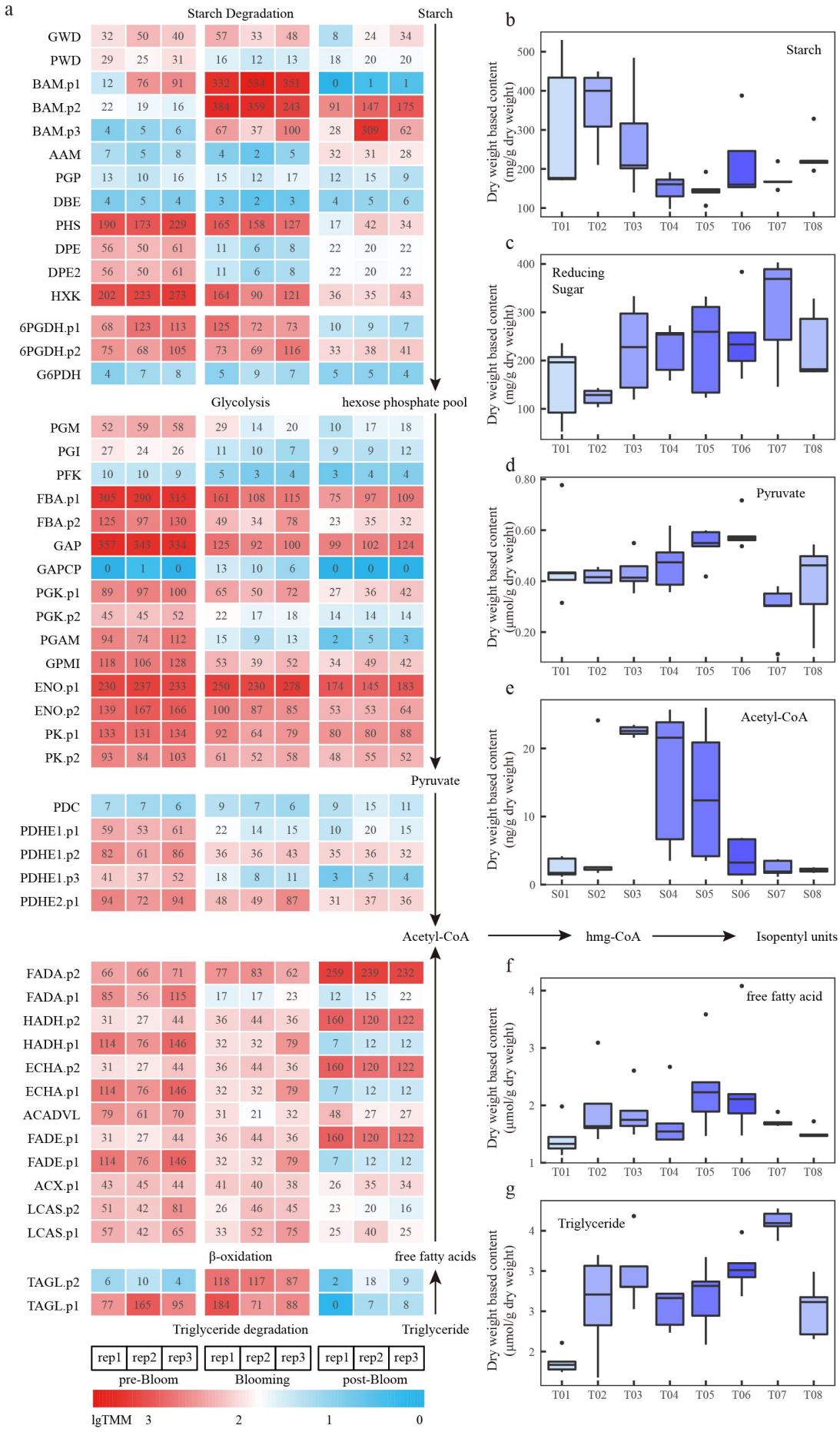
a
Starch Degradation
Starch
GWD 32 50 40 57 33 48 8 24 34
PWD 29 25 31 16 12 13 18 20 20
BAM.p1 12 76 91 332 534 351 0 1 1
BAM.p2 22 19 16 384 359 243 91 147 175
BAM.p3 4 5 6 67 37 100 28 309 62
AAM 7 5 8 4 2 5 32 31 28
PGP 13 10 16 15 12 17 12 15 9
DBE 4 5 4 3 2 3 4 5 6
PHS 190 173 229 165 158 127 17 42 34
DPE 56 50 61 11 6 8 22 20 22
DPE2 56 50 61 11 6 8 22 20 22
HXK 202 223 273 164 90 121 36 35 43
6PGDH.p1 68 123 113 125 72 73 10 9 7
6PGDH.p2 75 68 105 73 69 116 33 38 41
G6PDH 4 7 8 5 9 7 5 5 4
Glycolysis
hexose phosphate pool
PGM 52 59 58 29 14 20 10 17 18
PGI 27 24 26 11 10 7 9 9 12
PFK 10 10 9 5 3 4 3 4 4
FBA.p1 305 290 315 161 108 115 75 97 109
FBA.p2 125 97 130 49 34 78 23 35 32
GAP 357 343 334 125 92 100 99 102 124
GAPCP 0 1 0 13 10 6 0 0 0
PGK.p1 89 97 100 65 50 72 27 36 42
PGK.p2 45 45 52 22 17 18 14 14 14
PGAM 94 74 112 15 9 13 2 5 3
GPMI 118 106 128 53 39 52 34 49 42
ENO.p1 230 237 233 250 230 278 174 145 183
ENO.p2 139 167 166 100 87 85 53 53 64
PK.p1 133 131 134 92 64 79 80 80 88
PK.p2 93 84 103 61 52 58 48 55 52
Pyruvate
PDC 7 7 6 9 7 6 9 15 11
PDHE1.p1 59 53 61 22 14 15 10 20 15
PDHE1.p2 82 61 86 36 36 43 35 36 32
PDHE1.p3 41 37 52 18 8 11 3 5 4
PDHE2.p1 94 72 94 48 49 87 31 37 36
Acetyl-CoA
hmg-CoA
Isopentyl units
FADA.p2 66 66 71 77 83 62 259 239 232
FADA.p1 85 56 115 17 17 23 12 15 22
HADH.p2 31 27 44 36 44 36 160 120 122
HADH.p1 114 76 146 32 32 79 7 12 12
ECHA.p2 31 27 44 36 44 36 160 120 122
ECHA.p1 114 76 146 32 32 79 7 12 12
ACADVL 79 61 70 31 21 32 48 27 27
FADE.p1 31 27 44 36 44 36 160 120 122
FADE.p1 114 76 146 32 32 79 7 12 12
ACX.p1 43 45 44 41 40 38 26 35 34
LCAS.p2 51 42 81 26 46 45 23 20 16
LCAS.p1 57 42 65 33 52 75 25 40 25
β-oxidation
free fatty acids
TAGL.p2 6 10 4 118 117 87 2 18 9
TAGL.p1 77 165 95 184 71 88 0 7 8
Triglyceride degradation
Triglyceride
rep1 rep2 rep3 rep1 rep2 rep3 rep1 rep2 rep3
pre-Bloom
Blooming
post-Bloom
lgTMM 3 2 1 0
b
Starch
Dry weight based content (mg/g dry weight)
500 400 300 200 100
T01 T02 T03 T04 T05 T06 T07 T08
c
Reducing Sugar
Dry weight based content (mg/g dry weight)
400 300 200 100
T01 T02 T03 T04 T05 T06 T07 T08
d
Pyruvate
Dry weight based content (μmol/g dry weight)
0.80 0.60 0.40 0.20
T01 T02 T03 T04 T05 T06 T07 T08
e
Acetyl-CoA
Dry weight based content (ng/g dry weight)
20 10 0
S01 S02 S03 S04 S05 S06 S07 S08
f
free fatty acid
Dry weight based content (μmol/g dry weight)
4 3 2 1
T01 T02 T03 T04 T05 T06 T07 T08
g
Triglyceride
Dry weight based content (μmol/g dry weight)
4 3 3 2
T01 T02 T03 T04 T05 T06 T07 T08

669

670 **Fig. 7. Carbon source for trans-Geraniol biosynthesis in *Epiphyllum oxypetalum***
671 **petal**

672 (a): Expression pattern of starch degradation, glycolysis and β-oxidation pathway
673 genes at pre-Bloom (T03), Blooming (T06) and post-Bloom (T07), each block is
674 colored according to TMM value.

675 (b-g) Concentration of starch, reducing sugar, pyruvate, acetyl-CoA, free fatty acid
676 and triglyceride in petal at T01-T08.

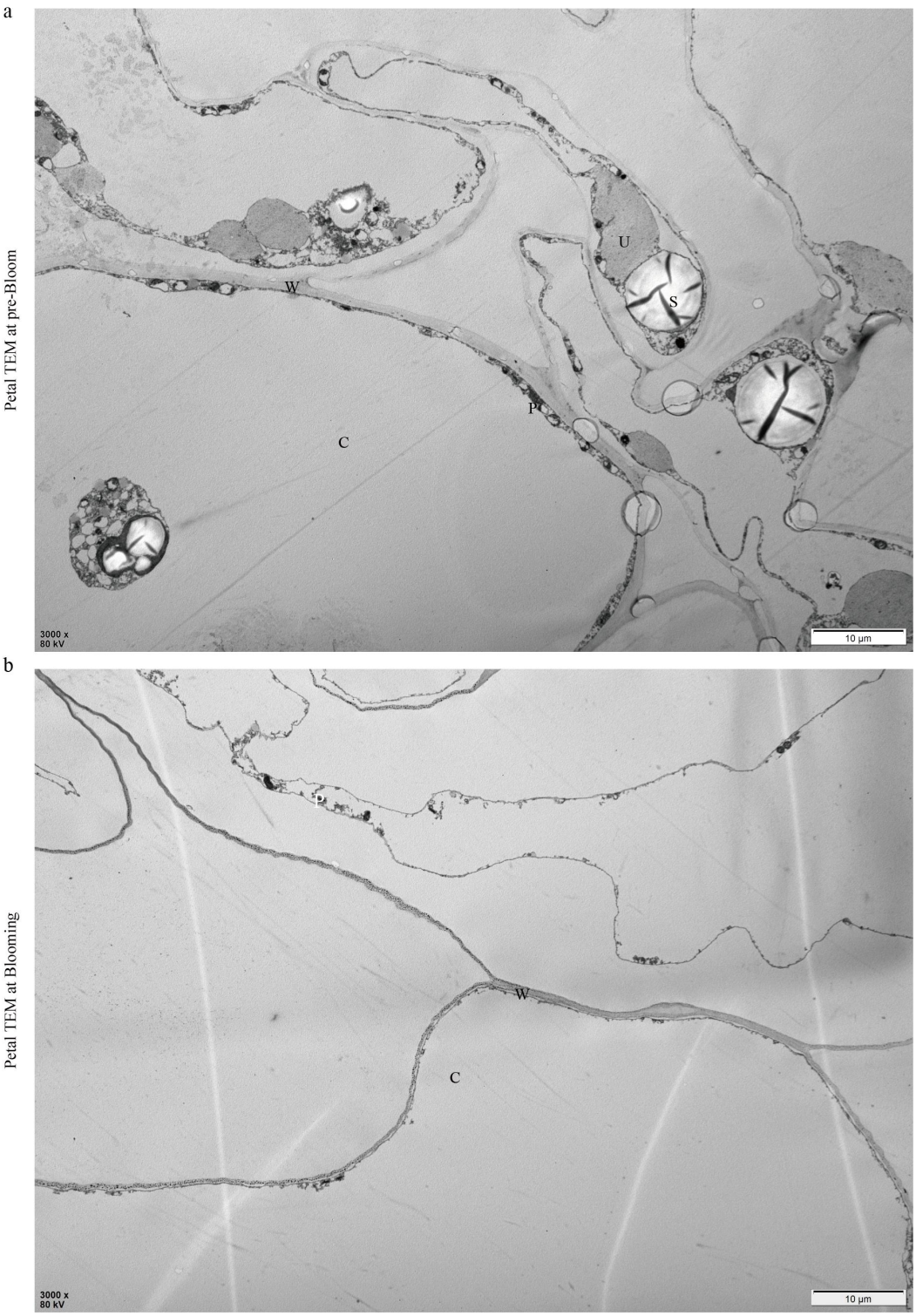

Fig. 8. TEM of *Epiphyllum oxypetalum* petal at pre-Bloom and Blooming stage

(a,b): TEM images of the petals of *E. oxypetalum* at pre-Bloom and Blooming stage. W, C, U, S represent cell wall， cytosol， unknown structure and starch granule respectively.

682 **Table 1.** Absolute emission rate of eight highest scent VOCs across 13 sampling Stages during *E. oxypetalum* flowering

VOC (μg/h)	trans-Geraniol	Benzyl alcohol	Methyl salicylate	trans-Citral	Benzyl salicylate	Benzyl benzoate	cis-Geraniol	Benzaldehyde	
RT/min	21.55	13.72	19.61	22.00	34.82	33.71	20.68	10.96	Total
Stage01	0.03 ± 0.01	0 ± 0	0.02 ± 0.01	0 ± 0	0.04 ± 0.01	0 ± 0	0.02 ± 0	0.04 ± 0.01	0.16 ± 0.02
Stage02	0.03 ± 0	0 ± 0	0.01 ± 0	0 ± 0	0.04 ± 0	0 ± 0	0.03 ± 0	0.05 ± 0	0.15 ± 0.01
Stage03	0.08 ± 0.04	0.01 ± 0.02	2.5 ± 1.57	0.01 ± 0.01	0.03 ± 0	0 ± 0	0.07 ± 0.02	0.05 ± 0	2.76 ± 1.66
Stage04	8.05 ± 2.67	0.39 ± 0.21	12.11 ± 1.92	0.35 ± 0.15	0.15 ± 0.06	0.18 ± 0.05	0.27 ± 0.08	0.2 ± 0.05	21.71 ± 4.51
Stage05	40.17 ± 7.77	2.42 ± 0.94	12.52 ± 2.32	1.28 ± 0.31	0.57 ± 0.13	0.94 ± 0.29	0.72 ± 0.17	0.52 ± 0.12	59.12 ± 11.23
Stage06	83.8 ± 3.64	7.95 ± 1.38	11 ± 0.31	2.67 ± 0.1	1.39 ± 0.4	1.57 ± 0.53	1.33 ± 0.08	1 ± 0.18	110.7 ± 4.98
Stage07	115.53 ± 12.62	16.28 ± 1.74	6.67 ± 0.96	3.45 ± 0.41	1.93 ± 0.89	1.39 ± 0.55	1.65 ± 0.3	1.35 ± 0.18	148.24 ± 16.58
Stage08	120.25 ± 16.1	22.84 ± 0.98	6.18 ± 0.8	2.68 ± 0.51	1.83 ± 0.41	0.9 ± 0.28	1.19 ± 0.21	1.6 ± 0.38	157.48 ± 18.7
Stage09	78.34 ± 24.16	25.02 ± 3.31	5.33 ± 0.5	1.29 ± 0.4	2.55 ± 0.9	0.59 ± 0.15	0.8 ± 0.17	1.28 ± 0.31	115.2 ± 29.43
Stage10	30.69 ± 13.24	20.6 ± 3.5	5.82 ± 0.74	0.52 ± 0.13	2.21 ± 1	0.36 ± 0.09	0.56 ± 0.08	0.78 ± 0.27	61.54 ± 17.97
Stage11	16.11 ± 2.09	0.85 ± 3.58	12.08 ± 3.66	0.58 ± 0.05	0.29 ± 0.65	0.32 ± 0.06	0.38 ± 0.06	0.29 ± 0.07	30.88 ± 3.18
Stage12	0.55 ± 0.24	2.15 ± 1.1	25.59 ± 2.28	0.03 ± 0.01	0.85 ± 0.39	0.1 ± 0.03	0.12 ± 0.04	0.11 ± 0.03	29.49 ± 3.94
Stage13	0.18 ± 0.06	0.76 ± 0.47	17.21 ± 7.21	0.02 ± 0.01	0.34 ± 0.15	0.07 ± 0.02	0.14 ± 0.07	0.08 ± 0.01	18.79 ± 7.75

683

684 **Table 2.** Relative content of 8 highest scent VOCs across 13 sampled Stages during *E. oxypetalum* flowering in percentage

VOC (%)	trans-Geraniol	Benzyl alcohol	Methyl salicylate	trans-Citral	Benzyl salicylate	Benzyl benzoate	cis-Geraniol	Benzaldehyde	
RT/min	21.55	13.72	19.61	22.00	34.82	33.71	20.68	10.96	Total
Stage01	4.02 ± 0.42	0 ± 0	2.2 ± 1.08	0 ± 0	5.76 ± 1.36	0.56 ± 0.12	3.14 ± 0.4	5.91 ± 0.36	21.59 ± 2.53
Stage02	4.35 ± 0.15	0 ± 0	1.65 ± 0.59	0 ± 0	5.1 ± 0.82	0.42 ± 0.12	4.06 ± 0.79	6.63 ± 0.24	22.21 ± 1.76
Stage03	2.37 ± 0.7	0.24 ± 0.34	70.16 ± 7.7	0.29 ± 0.15	1.24 ± 0.45	0.16 ± 0.05	2.32 ± 0.49	1.77 ± 0.68	78.55 ± 6.26
Stage04	33.35 ± 3.84	1.54 ± 0.49	52.13 ± 7.01	1.45 ± 0.29	0.69 ± 0.32	0.81 ± 0.27	1.1 ± 0.08	0.86 ± 0.14	91.92 ± 2.92
Stage05	63.56 ± 1.12	3.71 ± 0.76	19.95 ± 2.27	2.01 ± 0.08	0.94 ± 0.29	1.48 ± 0.37	1.13 ± 0.06	0.82 ± 0.12	93.6 ± 2.6
Stage06	72.55 ± 0.39	6.85 ± 0.94	9.54 ± 0.53	2.32 ± 0.18	1.2 ± 0.34	1.36 ± 0.45	1.15 ± 0.05	0.87 ± 0.16	95.83 ± 0.79
Stage07	74.47 ± 0.32	10.51 ± 0.61	4.28 ± 0.24	2.23 ± 0.13	1.22 ± 0.47	0.87 ± 0.26	1.06 ± 0.11	0.88 ± 0.15	95.54 ± 0.67
Stage08	72.54 ± 1.11	13.96 ± 1.38	3.75 ± 0.37	1.61 ± 0.17	1.09 ± 0.15	0.55 ± 0.18	0.72 ± 0.09	0.96 ± 0.15	95.18 ± 0.59
Stage09	62.16 ± 4.11	21.06 ± 3.62	4.55 ± 1	1.02 ± 0.07	1.99 ± 0.29	0.48 ± 0.04	0.66 ± 0.08	1.06 ± 0.19	92.99 ± 1.17
Stage10	43.02 ± 9.11	32.15 ± 5.2	9.75 ± 3.89	0.79 ± 0.07	3.07 ± 0.75	0.55 ± 0.1	0.96 ± 0.44	1.16 ± 0.17	91.45 ± 0.6
Stage11	43.63 ± 5.08	2.23 ± 7.02	41.38 ± 14.95	1.63 ± 0.12	0.83 ± 1.43	0.95 ± 0.14	1.12 ± 0.1	0.83 ± 0.13	92.6 ± 1.11
Stage12	1.72 ± 0.6	6.59 ± 2.99	83.96 ± 4.94	0.08 ± 0.03	2.68 ± 1.03	0.31 ± 0.07	0.37 ± 0.09	0.36 ± 0.04	96.07 ± 0.59
Stage13	0.95 ± 0.13	3.68 ± 1.33	85.99 ± 2.67	0.08 ± 0.02	2.06 ± 0.97	0.39 ± 0.11	0.71 ± 0.2	0.45 ± 0.17	94.32 ± 1.46

685

686 **Table 3.** Primers utilized in related experiments.

687

Experiment	Name	Sequences
qRT-PCR	2acat3f	TCGTCTTGGACATGATACAC
	2acat3r	ACTTCAACAGGAACCATCTC
	hmgcs10f	GATGGTCGTTATGGTCTGGT
	hmgcs10r	TCACTTATGGAGCTGGCATT
	hmg5f	CCTCAAATGTTTGGACCGAC
	hmg5r	AATCGACCTCCCTGTGATTC
	mvk8f	ACGTTGGAGAGCTAATCCTG
	mvk8r	AGGAAGCTCAGATGTCACAG
	mvak22f	TGTGCAATATTGTGTGGCAG
	mvak22r	ATGACCCCAAGCCTGTTTTA
	2mvad1f	ATACATCGCCGCCTATATTC
	2mvad1r	TTCCACATCTTTCGTGTCAT
	2idi5f	TTGGACGTATGCTCTACAAG
	2idi5r	CACTAGTCTGAACCATGGAG
	2dxps1f	TACTAAAACAACAGGTCCCG
	2dxps1r	TGCACAAAATGGTTTGAGAC
	dxr5f	ATCAGGCTCTACAACAGCTC
	dxr5r	GGCAAATTTGTGGGTTGAGT
	ispd6f	AATCTTGCTCCATAGAGGGC
	ispd6r	GGGGTGTCTCAAACCTTGTA
	ispe7f	GGCGGCGGAATATCTTTAAC
	ispe7r	TCAACAAATGTAGCTGGGGT
	ispf5f	GCATCTAAGTTGCCGAGTTC
	ispf5r	TTTCAGCAGTTTCGATCCCT
	2ispg1f	ATTATTGGGGGCATCAACAT
	2ispg1r	GACAAATTGGCCTTGATAGC
	isph5f	TACATGGGGTAACGTCACTG
	isph5r	AGTAGCTATGGTCTCCTCGT
	gdps7f	GTCTATGCCGTGCTCAAATC
	gdps7r	AGCCATTCTATACACCAGCC
	TPS-new4f	CTCTCTCATGCCAAGATATG
	TPS-new4r	GTGGGAATATAGCTGCATAG
	2ubqln8f	TGAGCCCAAATTATTACCTGCA
	2ubqln8r	ATACTCAATGACCCTAGCATTCT
E.coli expression	TPS-pETligf	atgggtcgcggatccATGTCGACTGATGATG
	TPS-pETligr	tgctcgagtgcggccgCTATGGAATGGGATGAAC
N. benthamiana expression	gdps-pSuper1300 ligf	catttaaatactagtATGAGCGATCTGAGGG
	gdps-pSuper1300 ligr	cgcccttgctcaccatATGAGAGTTGTC
	tps-pSuper1300 ligf	catttaaatactagtATGTCGACTGATGATGCAG
	tps-pSuper1300 ligr	cgcccttgctcaccatTGGAATGGGATGAACGAG